ACS APPLIED ENERGY MATERIALS

www.acsaem.org

Article

Ultrathin MnO_2 Sheet Arrays Grown on Hollow Carbon Fibers as Effective Polysulfide-Blocking Interlayers for High-Performance Li−S Batteries

Guojie Chao, Longsheng Zhang, Shijia Yuan, Tiantian Xue, Fan Yang, Yunpeng Huang, Wei Fan,* and Tianxi Liu

Cite This: *ACS Appl. Energy Mater.* 2020, 3, 12703−12708

Read Online

ACCESS | Metrics & More | Article Recommendations | Supporting Information

ABSTRACT: Lithium−sulfur (Li−S) batteries are clean energy conversion devices with high theoretical energy densities and specific capacities. However, Li−S batteries exhibit poor cycling stability during the practical test, mainly because of the detrimental shuttle effect of intermediate lithium polysulfides (LiPSs). Here, we report a common and scalable strategy to prepare freestanding membranes of MnO_2 sheet arrays anchored on natural cotton-derived hollow carbon fibers (MnO_2/HCFs), which as interlayers can mitigate shuttling of LiPSs and thus boost the durabilities of Li−S batteries. By combining ultraviolet−visible absorption and X-ray photoelectron spectroscopy, we find that a MnO_2/HCF interlayer can trap the LiPSs through chemical interactions between LiPSs and MnO_2. With a MnO_2/HCF interlayer, the Li−S battery shows a satisfactory capacity of 970 mA h g^{-1} at 1 A g^{-1} with a capacity decay of merely 0.12% per cycle over 500 cycles.

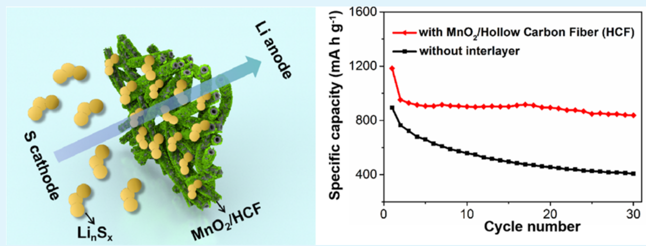

KEYWORDS: *lithium−sulfur batteries, polysulfide, interlayer, MnO_2, carbon fiber*

1. INTRODUCTION

The advancement of electronic and electrical devices has created a strong driving force for developing high energy density battery systems. Lithium−sulfur (Li−S) batteries are the environmentally friendly energy conversion devices with high theoretical energy density (2600 W h kg^{-1}) and specific capacity (1675 mA h g^{-1}), possessing great potential for practical application.[1−6] However, the practical application of Li−S batteries is appreciably limited because of the detrimental "shuttle effect" due to the dissolution and diffusion of lithium polysulfides (LiPSs).[7−11] Thus, breakthroughs in eliminating the "shuttle effect" of LiPSs are urgently desired.

To date, various works have been devoted to suppress the dissolution of LiPSs by optimizing the structure of cathodes and designing suitable composite materials as hosts for LiPSs.[12−14] Unfortunately, even with sulfur loading in these host cathodes, the dissolution and diffusion of LiPSs cannot be effectively hindered, thus resulting in the rapid battery capacity attenuation. To address this problem, besides designing host cathodes, employing effective polysulfide barriers as interlayers between the separator and cathode is a useful means to further hinder polysulfide shuttling. The interlayers, usually with porous and freestanding features, can work as second barriers to efficiently block the migration of LiPSs *via* physical or chemical interactions. Compared to other potential materials used as the interlayers in Li−S batteries, nanostructured metallic oxides, including TiO_2,[15] MnO_2,[16] and MoO_2,[17] have recently attracted great attention. Through chemical interaction, these oxides can efficiently trap the LiPSs to mitigate the polysulfide shuttling for promoting the durability of the Li−S battery. Meanwhile, the nanostructured oxides agglomerate easily, which will reduce the utilization of materials. Moreover, these oxides also have the property of low conductivity, boosting the internal charge transfer resistance.[18]

Herein, we demonstrate a facile and scalable process to prepare a freestanding hybrid membrane of ultrathin MnO_2 sheet arrays grown on hollow carbon fibers (HCFs), which as an interlayer can efficiently restrain the shuttling of LiPSs and increase the durability of the Li−S battery. The HCF skeleton can work as the 3D interconnected conductive network for promoting both electron and ion transport during the charging and discharging process. Meanwhile, the HCF is derived from carbonizing natural cotton, which is cost-effective and eco-friendly. The hollow structure of HCFs enables the ready access of LiPSs with the well-dispersed MnO_2 sheet arrays that are grown on both the inside and outside wall of HCFs, which can help to anchor LiPSs and retard polysulfide shuttling by

Received: October 28, 2020
Accepted: December 2, 2020
Published: December 15, 2020

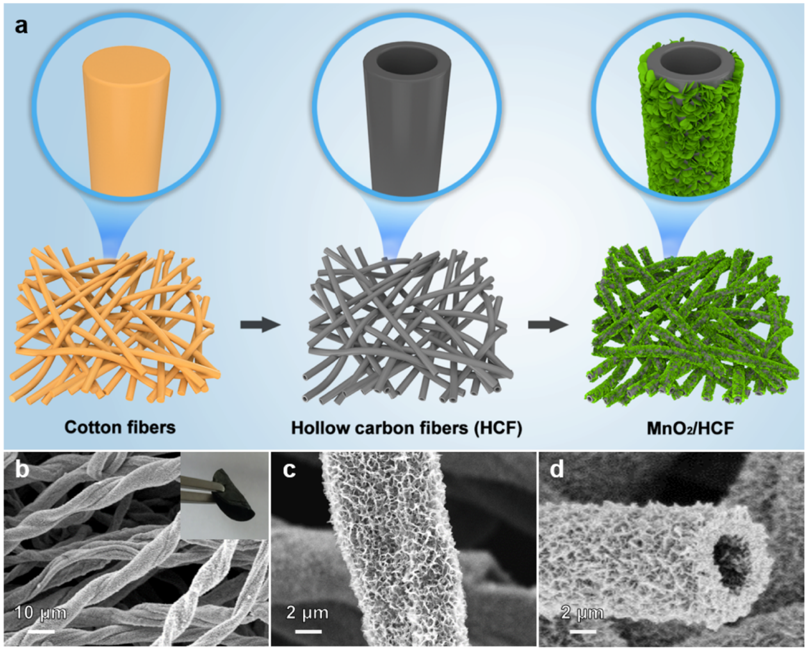

Figure 1. (a) Schematic illustration for preparing the MnO_2/HCF interlayer. (b−d) SEM images of the MnO_2/HCF interlayer. The inset of (b) is the photograph of the MnO_2/HCF membrane.

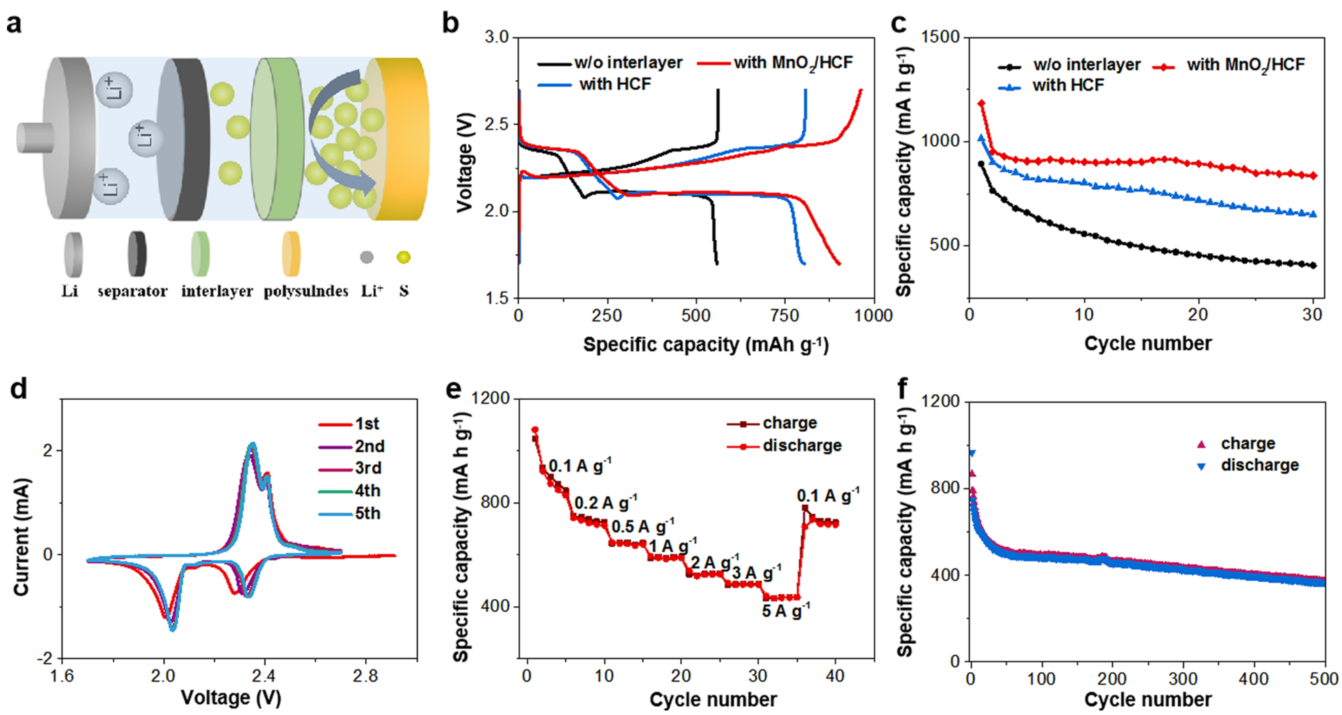

Figure 2. (a) Schematic of the Li−S battery assembled with a polysulfide-blocking interlayer. (b) Charge/discharge voltage curves of the Li−S battery without the interlayer and with the HCF or MnO_2/HCF interlayer at a current density of 0.1 A g^{-1}. (c) Galvanostatic charge/discharge profiles of the Li−S battery at 0.1 A g^{-1}. (d) CV profiles and (e) rate performance of the Li−S battery with the MnO_2/HCF interlayer. (f) Cycling test of the Li−S battery with the MnO_2/HCF interlayer at 1 A g^{-1}.

chemical interactions. Ultraviolet−visible (UV−vis) absorption spectroscopy, combined with X-ray photoelectron spectroscopy (XPS), provides solid evidence for the effective chemical absorption between MnO_2 and LiPSs. Assembling with this ingenious MnO_2/HCF interlayer, the Li−S battery shows an excellent capacity of 970 mA h g^{-1} at 1 A g^{-1} with a lower capacity decay of only 0.12% per cycle over 500 cycles.

2. RESULTS AND DISCUSSION

As illustrated in Figure 1a, the MnO_2/HCF membrane was prepared by modifying MnO_2 sheet arrays on HCFs by the one facile hydrothermal method. HCFs were first prepared by carbonizing natural cotton fibers at a high temperature (Figures S1 and S2). As shown in the scanning electron microscopy (SEM) images (Figure 1b,c), it is demonstrated

https://dx.doi.org/10.1021/acsaem.0c02672
ACS Appl. Energy Mater. 2020, 3, 12703−12708

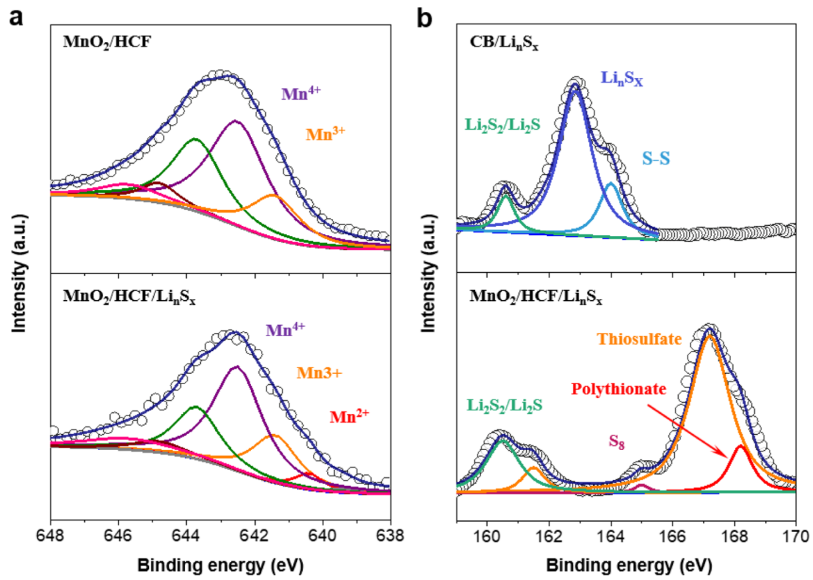

Figure 3. (a) High-resolution Mn 2p spectra of the MnO_2/HCF interlayer before and after 100 cycles. (b) High-resolution S 2p spectra of cathode materials of the battery with and without the MnO_2/HCF interlayer after 100 cycles.

that ultrathin MnO_2 sheet arrays are uniformly grown on the surface of HCFs. Besides, MnO_2 sheets can even be grown on the inner wall of HCFs (Figure 1d). From the transmission electron microscopy (TEM) images of MnO_2/HCF (Figure S3), it can also be seen that MnO_2 sheets are grown on the HCF fibers. The high-resolution TEM image reveals the (001) and (110) crystal planes of MnO_2 (Figure S3b). The content of MnO_2 in the MnO_2/HCF membrane is 7.5% (Figure S4), obtained from the thermogravimetry (TG) analysis. The areal loading of MnO_2 in the MnO_2/HCF membrane is 0.14 μg mm^{-2}. The resulting MnO_2/HCF membrane is freestanding with a thickness of ~0.35 mm (inset of Figure 1b), which can be cut into desirable shapes. According to the X-ray diffraction pattern (Figure S5), MnO_2 of the MnO_2/HCF membrane can be ascribed to δ-MnO_2 (JCPDS card no. 80-1098), which would provide efficient adsorption of LiPS species by chemical interaction.[19] As displayed in Figure S6, after the MnO_2/HCF membrane was immersed into the Li_2S_4 solution, the solution began to fade and became almost colorless after 2 h. By contrast, no noticeable change in color was observed for the Li_2S_4 solution with the HCF membrane. These results indicate the superior adsorbent ability of LiPS species for the MnO_2/HCF membrane. We further conducted the UV−vis absorption test to investigate the content of LiPS species in the electrolyte with and without the MnO_2/HCF membrane. In the UV−vis absorption spectra (Figure S7), three peaks at 280, 310, and 422 nm are observed for Li_2S_4 solution without the MnO_2/HCF membrane, which can be labeled as S_8/S_6^{2-}, S_6^{2-}/S_4^{2-}, and S_4^{2-} species, respectively.[20,21] For Li_2S_4 solution with the MnO_2/HCF membrane, hardly any S_4^{2-} species can be seen and the concentrations of S_8 and S_6^{2-} species are much lower, which verifies that the MnO_2/HCF membrane has appreciable adsorption of LiPS species.

To further evaluate the effect of blocking polysulfide for MnO_2/HCF interlayers, we conducted the electrochemical measurement by assembling Li−S batteries with the MnO_2/HCF interlayers. As illustrated in Figure 2a, the MnO_2/HCF interlayers were placed between the separator and the cathode. As shown in Figure 2b, the charge/discharge profiles of Li−S batteries show two major plateaus at 2.34 and 2.10 V because of the conversion of S_8 to long-chain LiPSs and to Li_2S, respectively.[22,23] Compared with Li−S batteries without the interlayer or with the HCF, the battery with the MnO_2/HCF interlayer exhibits higher upper-plateau and lower-plateau discharge capacities. The battery with the MnO_2/HCF interlayer exhibits higher electrochemical performance than those with HCF interlayers or without interlayers (Figure 2c). After 30 cycles, the battery with the MnO_2/HCF interlayer retains satisfactory discharge capacity (837 mA h g^{-1}), which is higher than that with the HCF (649 mA h g^{-1}) or without the interlayer (406 mA h g^{-1}). Assuredly, the MnO_2/HCF interlayer is beneficial to promote the electrochemical performance of the Li−S battery, which can restrict the shuttling of the polysulfides and prevent capacity decay.

As shown in the CV curves of the Li−S battery with MnO_2/HCF (Figure 2d), two reduction peaks correspond to the reversible transition of S_8 into long-chain LiPSs and finally to Li_2S, while the anodic peaks correspond to the conversion from Li_2S to LiPSs and S_8.[24−28] Also, these curves are nearly overlapped after the first cycle, exhibiting good stability and reversibility of the battery. The rate capability of the Li−S battery with the MnO_2/HCF interlayer was investigated under different cycling rates from 0.1 to 5 A g^{-1} (Figure 2e). Specifically, the Li−S battery with the MnO_2/HCF interlayer exhibits remarkable capacities of 1081, 748, 647, 591, 526, 488, and 438 mA h g^{-1} at 0.1, 0.2, 0.5, 1, 2, 3, and 5 A g^{-1}. The charge/discharge plateaus of voltage curves in galvanostatic profiles are stable with negligible change from 0.1 to 5 A g^{-1} (Figure S8). Notably, nearly 70% of the original capacity (753 mA h g^{-1}) was retained when the current density returned to 0.1 A g^{-1}, indicating that the MnO_2/HCF interlayer can effectively prevent capacity decay and promote the durability of the Li−S battery. According to the long-term cycling test (Figure 2f), the Li−S battery with MnO_2/HCF exhibits lower capacity decay of 0.12% per cycle. Notably, the battery suffers from rapid capacity decay in the initial cycles. As reported, part of sulfur in the cathode will be transformed into LiPSs, which will cause capacity decay in the initial cycles.[29,30] In addition, the shuttle effect of LiPSs cannot be totally avoided, which would also cause capacity decay of the batteries. To better

https://dx.doi.org/10.1021/acsaem.0c02672
ACS Appl. Energy Mater. 2020, 3, 12703−12708

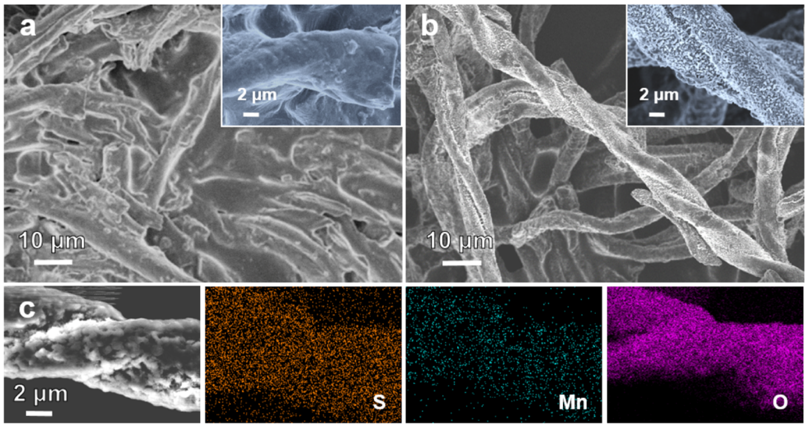

Figure 4. SEM images of (a) HCF interlayer and (b) MnO_2/HCF interlayer after 100 cycles. (c) Elemental mapping images of the MnO_2/HCF interlayer after 100 cycles.

understand the interaction between MnO_2 and Li_xS_n species, we have further conducted XPS for the MnO_2/HCF interlayer before and after 100 cycles in the Li−S battery (Figure 3). As shown in Figure 3a, in the high-resolution Mn 2p spectra, it is observed that the intensity of the Mn^{3+} peak greatly increases after discharge. Besides, one extra peak located at 640.4 eV is marked as the XPS peak of Mn^{2+} reduced from the Mn^{4+}/Mn^{3+}, which is derived by the oxidation of Li_xS_n species.[31] As shown in the high-resolution S 2p spectra (Figure 3b), there are three peaks at 164.0, 162.9, and 160.2 eV in the spectrum of the Li−S battery without the interlayer. The peak at 164.0 eV is attributed to the S−S bond.[31] The presence of Li_xS_n ($3 \leq n \leq 8$) is verified by the strong S $2p_{3/2}$ contribution at 162.9 eV, and the XPS peak at 160.2 eV corresponds to the Li−S bonds of Li_2S_2 and Li_2S deposited in the sulfur cathode.[32,33] In the high-resolution S 2p spectrum of the Li−S battery with the MnO_2/HCF interlayer, a strong peak at 167.2 eV can be ascribed to the central S═O bond of thiosulfate captured by the surface redox reaction between Li_xS_n ($3 \leq n \leq 8$) and δ-MnO_2, along with its peripheral S peak at 161.5 eV.[34] The new peak at 165.0 eV is attributed to S_8 species.[35,36] As reported, the longer-chain polysulfide can react with thiosulfate species to generate shorter polysulfide and polythionate complexes (Figure S9).[19] The strong peak at 168.2 eV can be attributed to the polythionate complex of MnO_2−Li_xS_n ($3 \leq n \leq 8$). These results, taken together, verify the chemical interaction between δ-MnO_2 and polysulfides, which will be beneficial for inhibiting diffusion of Li_xS_n and rapid capacity decay.

We have carried out the postmortem morphological analysis of HCF and MnO_2/HCF interlayers of the Li−S battery after long-term cycling to further investigate their structural stability. As shown in the SEM images of the HCF, it is observed that the sulfurs and polysulfides aggregate unevenly onto the HCF membranes after the long-term cycling process. In sharp contrast, the sulfurs and polysulfides are uniformly deposited onto the surfaces of MnO_2/HCF hybrid fibers. Also, the nanostructures of the MnO_2/HCF interlayer are well maintained after long-term cycling tests (Figures 4b and S10). Moreover, as shown in Figure 4c, Mn, O, and S elements are homogeneously distributed onto the hybrid fibers of the MnO_2/HCF interlayer, which verifies that sulfurs and polysulfides can be captured by the MnO_2/HCF interlayer during the charge/discharge process. In conjunction with electrochemical results and XPS studies, the enhanced cycling stability with the MnO_2/HCF interlayer is due to effectively capturing polysulfides by δ-MnO_2 and restricting the shuttling of polysulfides by the MnO_2/HCF hybrid interlayer.

3. CONCLUSIONS

In summary, we demonstrate a facile and scalable strategy to obtain MnO_2/HCF membranes with MnO_2 sheet arrays grown on natural cotton-derived HCFs. The hollow structure of HCFs can facilitate the access of LiPSs with the MnO_2 sheet arrays that are grown on both the inside and outside wall of HCFs. The strong chemical interactions formed between MnO_2 and LiPSs can helpfully mitigate the shuttling of LiPSs, as verified by the UV−vis and XPS measurements. Assembling with the well-designed MnO_2/HCF interlayer, the Li−S battery shows excellent capacity at high current density and exhibits satisfactory cycling stability with a capacity decay of merely 0.12% per cycle during the cyclic test.

4. EXPERIMENTAL SECTION

4.1. Materials. Cotton papers were purchased from Shenzhen PurCotton Technology. The carbon black and sulfur were bought from Alfa Aesar. $KMnO_4$ was purchased from Sinopharm Chemical Reagents. Poly(vinylidene fluoride) was obtained from Sigma-Aldrich. The electrolyte was purchased from Xiaoyuan Energy Technology. All reagents were used without further purification.

4.2. Synthesis of HCF and MnO_2/HCF Interlayers. HCF membranes were prepared by pyrolyzing cotton membranes at 900 °C for 2 h under an Ar atmosphere in a tube furnace. Afterward, ultrathin MnO_2 sheet arrays were grown on the HCF *via* a facile solvothermal method. Then, 70 mL of $KMnO_4$ solution (0.8 mmol L^{-1}) was slowly added to deionized water (700 mL) under stirring. The HCF membranes were immersed into the solution in a watch glass. After heat treatment at 80 °C for 10 h, the MnO_2/HCF membranes were obtained after washing with deionized water and drying in a vacuum oven at 60 °C for 12 h.

■ ASSOCIATED CONTENT

Supporting Information

The Supporting Information is available free of charge at https://pubs.acs.org/doi/10.1021/acsaem.0c02672.

Characterization and electrochemical measurements; XRD patterns of HCF and MnO_2/HCF; TEM images of HCF and MnO_2/HCF; TGA measurements of HCF and MnO_2/HCF; UV−vis absorption tests of the LiPSs; and galvanostatic charge/discharge profiles at various current densities (PDF)

https://dx.doi.org/10.1021/acsaem.0c02672
ACS Appl. Energy Mater. 2020, 3, 12703−12708

AUTHOR INFORMATION

Corresponding Author

Wei Fan − *State Key Laboratory for Modification of Chemical Fibers and Polymer Materials College of Materials Science and Engineering, Innovation Center for Textile Science and Technology, Donghua University, Shanghai 201620, P. R. China;* orcid.org/0000-0001-6978-1405; Email: weifan@dhu.edu.cn

Authors

Guojie Chao − *State Key Laboratory for Modification of Chemical Fibers and Polymer Materials College of Materials Science and Engineering, Innovation Center for Textile Science and Technology, Donghua University, Shanghai 201620, P. R. China*

Longsheng Zhang − *Key Laboratory of Synthetic and Biological Colloids, Ministry of Education, School of Chemical and Material Engineering, Jiangnan University, Wuxi 214122, P. R. China*

Shijia Yuan − *State Key Laboratory for Modification of Chemical Fibers and Polymer Materials College of Materials Science and Engineering, Innovation Center for Textile Science and Technology, Donghua University, Shanghai 201620, P. R. China*

Tiantian Xue − *State Key Laboratory for Modification of Chemical Fibers and Polymer Materials College of Materials Science and Engineering, Innovation Center for Textile Science and Technology, Donghua University, Shanghai 201620, P. R. China*

Fan Yang − *State Key Laboratory for Modification of Chemical Fibers and Polymer Materials College of Materials Science and Engineering, Innovation Center for Textile Science and Technology, Donghua University, Shanghai 201620, P. R. China*

Yunpeng Huang − *Key Laboratory of Synthetic and Biological Colloids, Ministry of Education, School of Chemical and Material Engineering, Jiangnan University, Wuxi 214122, P. R. China*

Tianxi Liu − *State Key Laboratory for Modification of Chemical Fibers and Polymer Materials College of Materials Science and Engineering, Innovation Center for Textile Science and Technology, Donghua University, Shanghai 201620, P. R. China; Key Laboratory of Synthetic and Biological Colloids, Ministry of Education, School of Chemical and Material Engineering, Jiangnan University, Wuxi 214122, P. R. China*

Complete contact information is available at: https://pubs.acs.org/10.1021/acsaem.0c02672

Notes

The authors declare no competing financial interest.

ACKNOWLEDGMENTS

The authors are grateful for Shanghai Scientific and Technological Innovation Project (18JC1410600), the Fundamental Research Funds for the Central Universities (2232017D-06, 2232019A3-03), the financial support from the National Natural Science Foundation of China (21704014), Program of Shanghai Academic Research Leader (17XD1400100), Shanghai Municipal Education Commission (17CG33), and Shanghai Sailing Program (17YF1400200).

REFERENCES

(1) Bruce, P. G.; Freunberger, S. A.; Hardwick, L. J.; Tarascon, J. M. Li-O_2 and Li-S batteries with high energy storage. *Nat. Mater.* **2012**, *11*, 19−29.

(2) Zhang, C.; Wu, H. B.; Yuan, C.; Guo, Z.; Lou, X. W. D. Confining sulfur in double-shelled hollow carbon spheres for lithium-sulfur batteries. *Angew. Chem., Int. Ed.* **2012**, *51*, 9592−9595.

(3) Zeng, L.; Pan, F.; Li, W.; Jiang, Y.; Zhong, X.; Yu, Y. Free-standing porous carbon nanofibers-sulfur composite for flexible Li-S battery cathode. *Nanoscale* **2014**, *6*, 9579−9587.

(4) Pang, Q.; Shyamsunder, A.; Narayanan, B.; Kwok, C. Y.; Curtiss, L. A.; Nazar, L. F. Tuning the electrolyte network structure to invoke quasi-solid-state sulfur conversion and suppress lithium dendrite formation in Li-S batteries. *Nat. Energy* **2018**, *3*, 783−791.

(5) He, J.; Hartmann, G.; Lee, M.; Hwang, G. S.; Chen, Y.; Manthiram, A. Freestanding 1T MoS_2/graphene heterostructures as a highly efficient electrocatalyst for lithium polysulfides in Li-S batteries. *Energy Environ. Sci.* **2019**, *12*, 344−350.

(6) Fan, W.; Zhang, L.; Liu, T. Multifunctional second barrier layers for lithium-sulfur batteries. *Mater. Chem. Front.* **2018**, *2*, 235.

(7) Niu, S.; Lv, W.; Zhang, C.; Shi, Y.; Zhao, J.; Li, B.; Yang, Q.-H.; Kang, F. One-pot self-assembly of graphene/carbon nanotube/sulfur hybrid with three dimensionally interconnected structure for lithium-sulfur batteries. *J. Power Sources* **2015**, *295*, 182−189.

(8) Fei, L.; Li, X.; Bi, W.; Zhuo, Z.; Wei, W.; Sun, L.; Lu, W.; Wu, X.; Xie, K.; Wu, C.; Chan, H. L. W.; Wang, Y. Graphene/sulfur hybrid nanosheets from a space-confined "sauna" reaction for high-performance lithium-sulfur batteries. *Adv. Mater.* **2015**, *27*, 5936−5942.

(9) Liu, M.; Zhou, D.; He, Y.-B.; Fu, Y.; Qin, X.; Miao, C.; Du, H.; Li, B.; Yang, Q.-H.; Lin, Z.; Zhao, T. S.; Kang, F. Novel gel polymer electrolyte for high-performance lithium-sulfur batteries. *Nano Energy* **2016**, *22*, 278−289.

(10) Park, J.; Yu, B.-C.; Park, J. S.; Choi, J. W.; Kim, C.; Sung, Y.-E.; Goodenough, J. B. Tungsten disulfide catalysts supported on a carbon cloth interlayer for high performance Li-S battery. *Adv. Energy Mater.* **2017**, *7*, 1602567.

(11) Wang, Y.; Zhang, R.; Pang, Y.-c.; Chen, X.; Lang, J.; Xu, J.; Xiao, C.; Li, H.; Xi, K.; Ding, S. Carbon@titanium nitride dual shell nanospheres as multi-functional hosts for lithium sulfur batteries. *Energy Storage Mater.* **2019**, *16*, 228−235.

(12) Shen, J.; Feng, Y.; Wang, P.; Qiu, G.; Zhang, L.; Lu, L.; Wang, H.; Wang, R.; Linkov, V.; Ji, S. Conductive sulfur-rich copolymer composites as lithium-sulfur battery electrodes with fast kinetics and a high cycle stability. *ACS Sustainable Chem. Eng.* **2020**, *8*, 10389−10401.

(13) Ding, G.; Li, Y.; Zhang, Y.; Huang, C.; Yao, X.; Lin, K.; Shen, K.; Yan, W.; Sun, F.; Zhou, L. Waste to wealth: Exhausted nitrogen-doped mesoporous carbon/MgO desulfurizers turned to high-sulfur-loading composite cathodes for Li-S batteries. *ACS Appl. Mater. Interfaces* **2019**, *11*, 19096−19103.

(14) Li, J.; Wei, W.; Meng, L. Liquid-phase exfoliated-graphene-supporting nanostructural sulfur as high-performance lithium-sulfur batteries cathode. *Compos. Commun.* **2019**, *15*, 149−154.

(15) Guo, J.; Zhao, S.; Shen, Y.; Shao, G.; Zhang, F. "Room-like" TiO_2 array as a sulfur host for lithium-sulfur batteries: Combining advantages of array and closed structures. *ACS Sustainable Chem. Eng.* **2020**, *8*, 7609−7616.

(16) Li, Z.; Zhang, J.; Lou, X. W. D. Hollow carbon nanofibers filled with MnO_2 nanosheets as efficient sulfur hosts for lithium-sulfur batteries. *Angew. Chem., Int. Ed.* **2015**, *54*, 12886−12890.

(17) Wang, C.; Li, K.; Zhang, F.; Wu, Z.; Sun, L.; Wang, L. Insight of enhanced redox chemistry for porous MoO_2 carbon derived framework as polysulfide reservoir in lithium-sulfur batteries. *ACS Appl. Mater. Interfaces* **2018**, *10*, 42286−42293.

(18) Niu, S.; Lv, W.; Zhou, G.; Shi, H.; Qin, X.; Zheng, C.; Zhou, T.; Luo, C.; Deng, Y.; Li, B.; Kang, F.; Yang, Q.-H. Electrostatic-spraying an ultrathin, multifunctional and compact coating onto a cathode for a

long-life and high-rate lithium-sulfur battery. *Nano Energy* **2016**, *30*, 138−145.
(19) Liang, X.; Hart, C.; Pang, Q.; Garsuch, A.; Weiss, T.; Nazar, L. F. A highly efficient polysulfide mediator for lithium-sulfur batteries. *Nat. Commun.* **2015**, *6*, 5682.
(20) Li, Y.; Zhan, H.; Liu, S.; Huang, K.; Zhou, Y. Electrochemical properties of the soluble reduction products in rechargeable Li/S battery. *J. Power Sources* **2010**, *195*, 2945−2949.
(21) Barchasz, C.; Molton, F.; Duboc, C.; Leprêtre, J.-C.; Patoux, S.; Alloin, F. Lithium/sulfur cell discharge mechanism: an original approach for intermediate species identification. *Anal. Chem.* **2012**, *84*, 3973−3980.
(22) Babu, D. B.; Ramesha, K. Melamine assisted liquid exfoliation approach for the synthesis of nitrogen doped graphene-like carbon nano sheets from bio-waste bagasse material and its application towards high areal density Li-S batteries. *Carbon* **2019**, *144*, 582−590.
(23) Huang, S.; Zhang, L.; Wang, J.; Zhu, J.; Shen, P. K. In situ carbon nanotube clusters grown from three dimensional porous graphene networks as efficient sulfur hosts for high-rate ultra-stable Li-S batteries. *Nano Res.* **2018**, *11*, 1731−1743.
(24) Xu, R.; Belharouak, I.; Li, J. C. M.; Zhang, X.; Bloom, I.; Bareño, J. Role of polysulfides in self-healing lithium-sulfur batteries. *Adv. Energy Mater.* **2013**, *3*, 833−838.
(25) Zhang, C.; Lv, W.; Zhang, W.; Zheng, X.; Wu, M.-B.; Wei, W.; Tao, Y.; Li, Z.; Yang, Q.-H. Reduction of graphene oxide by hydrogen sulfide: A promising strategy for pollutant control and as an electrode for Li-S batteries. *Adv. Energy Mater.* **2014**, *4*, 1301565.
(26) Yeon, J. S.; Yun, S.; Park, J. M.; Park, H. S. Surface-modified sulfur nanorods immobilized on radially assembled open-porous graphene microspheres for lithium-sulfur batteries. *ACS Nano* **2019**, *13*, 5163−5171.
(27) Yao, W.; Liu, L.; Wu, X.; Qin, C.; Xie, H.; Su, Z. Polyoxometalates/active carbon thin separator for improving cycle performance of lithium-sulfur batteries. *ACS Appl. Mater. Interfaces* **2018**, *10*, 35911−35918.
(28) Mao, J.; Wu, J.; Shi, W.; Liu, W.; Xu, X.; Cai, G.; Li, Y.; Cao, X. Preparation of polyaniline-coated composite aerogel of MnO_2 and reduced graphene oxide for high-performance Zinc-ion battery. *Chin. J. Polym. Sci.* **2019**, *38*, 514.
(29) Xu, G.; Yuan, J.; Tao, X.; Ding, B.; Dou, H.; Yan, X.; Xiao, Y.; Zhang, X. Absorption mechanism of carbon-nanotube paper titanium dioxide as a multifunctional barrier material for lithium-sulfur batteries. *Nano Res.* **2015**, *8*, 3066−3074.
(30) Cuisinier, M.; Cabelguen, P.-E.; Evers, S.; He, G.; Kolbeck, M.; Garsuch, A.; Bolin, T.; Balasubramanian, M.; Nazar, L. F. Sulfur speciation in Li-S batteries determined by operando X-ray absorption spectroscopy. *J. Phys. Chem. Lett.* **2013**, *4*, 3227−3232.
(31) Demir-Cakan, R.; Morcrette, M.; Nouar, F.; Davoisne, C.; Devic, T.; Gonbeau, D.; Dominko, R.; Serre, C.; Férey, G.; Tarascon, J.-M. Cathode composites for Li-S batteries via the use of oxygenated porous architectures. *J. Am. Chem. Soc.* **2011**, *133*, 16154−16160.
(32) Ota, H.; Sakata, Y.; Wang, X.; Sasahara, J.; Yasukawa, E. Characterization of lithium electrode in lithium imides/ethylene carbonate and cyclic ether electrolytes II. Surface chemistry. *J. Electrochem. Soc.* **2004**, *151*, A437−A446.
(33) Li, Y.; Cai, Q.; Wang, L.; Li, Q.; Peng, X.; Gao, B.; Huo, K.; Chu, P. K. Mesoporous TiO_2 nanocrystals/graphene as an efficient sulfur host material for high-performance lithium-sulfur batteries. *ACS Appl. Mater. Interfaces* **2016**, *8*, 23784−23792.
(34) Lindberg, B. J.; Hamrin, K.; Johansson, G.; Gelius, U.; Fahlman, A.; Nordling, C.; Siegbahn, K. Molecular spectroscopy by means of ESCA II. sulfur compounds. Correlation of electron binding energy with structure. *Phys. Scr.* **1970**, *1*, 286−298.
(35) Tian, Z.; Li, J.; Zhu, G.; Lu, J.; Wang, Y.; Shi, Z.; Xu, C. Facile synthesis of highly conductive sulfur-doped reduced graphene oxide sheets. *Phys. Chem. Chem. Phys.* **2016**, *18*, 1125−1130.
(36) Ma, L.; Zhuang, H. L.; Wei, S.; Hendrickson, K. E.; Kim, M. S.; Cohn, G.; Hennig, R. G.; Archer, L. A. Enhanced Li-S batteries using amine-functionalized carbon nanotubes in the cathode. *ACS Nano* **2016**, *10*, 1050−1059.

https://dx.doi.org/10.1021/acsaem.0c02672
ACS Appl. Energy Mater. 2020, 3, 12703−12708